THE EUROPEAN
PHYSICAL JOURNAL PLUS

Different methods for the identification of short-life nuclei: the ^{8}Be case

Cardella Giuseppe[1,a] (ID)**, Gnoffo Brunilde**[1,2,b]**, Acosta Luis**[4,6]**, De Filippo Enrico**[1]**, Geraci Elena**[1,2]**, Guazzoni Chiara**[4]**,
Maiolino Concetta**[3]**, Martorana Nunzia Simona**[2,3]**, Pagano Angelo**[1]**, Pagano Emanuele Vincenzo**[3]**, Papa Massimo**[1]**,
Pirrone Sara**[1]**, Politi Giuseppe**[1,2]**, Risitano Fabio**[1,5]**, Rizzo Francesca**[2,3]**, Russotto Paolo**[3]**, Trimarchí Marina**[1,5]

[1] INFN Sezione di Catania, Catania, Italy
[2] Dipartimento di Fisica e Astronomia "Ettore Majorana", Università di Catania, Catania, Italy
[3] Laboratori Nazionali del Sud, INFN, Catania, Italy
[4] DEIB, Politecnico di Milano and INFN Sezione di Milano, Milano, Italy
[5] Dipartimento di Scienze MIFT, Università di Messina, Messina, Italy
[6] Instituto de Física, Universidad Nacional Autónoma de México, Mexico city, Mexico

Abstract We show all different detection methods for ^{8}Be identification, available in the 4π CHIMERA multidetector. The methods here presented are interesting because they can be extended to resonances also in radioactive nuclei at the border of drip lines, in reactions in inverse kinematics that are characterized by small relative angles among the decay products. In particular, an analysis of the kinematic detection method is done by discussing the effect of the angular resolution on the accuracy determination of the energy of the resonance. Various "pile up" identification methods are shown, as the well known ΔE-E method, the time of flight technique and pulse shape analysis. The last section is focused on simulations, that show how the energy is shared between α-particles emitted by a ^{8}Be nucleus. A method that tries to recover for the limits in detector angular resolution is also described by investigating its possibilities and uncertainties.

1 Introduction

The isospin symmetry of nuclear forces is quite evident in light nuclei for which the stability valley is centered on the equal value of the neutron (N) and proton (Z) numbers. This symmetry is broken in the case of $Z = 4$ isotopes that need one more neutron to form the stable isotope ^{9}Be. So ^{8}Be is the only unstable light nucleus with N=Z. The very small resonance energy of the ground state (GS) of such a nucleus, approximately 92 keV [1], and its short life time produce important effects, specially in the stars where they play a crucial role in the ^{12}C production [2, 3]. The peculiar behaviour of this resonance induced in the past the development of various detection techniques. The different techniques can be grouped in two main species, the first one is based on kinematic methods [4–10] and the second one on "pile-up" methods [8, 11, 12]. The kinematic methods are generally more accurate, and they are based on the detection and identification of both decaying α-particles, where the excitation energy of the emitting nucleus is calculated from the reaction kinematics. Various examples can be found in the literature, as a very recent one, in which the accurate position reconstruction of ^{8}Be events with emulsions [10] was used also at relativistic energy. In the literature also works with dedicated multi-detector arrays [4, 5, 13, 14], or drift chambers, for a more precise position measurement [6] or using silicon strip detectors [7] and position sensitive detectors [8] are available.

The "pile-up" methods are usually characterized by a larger ^{8}Be detection efficiency, and they can be used as channel selection methods for nuclear structure measurements, as for instance it was done in the past years using the ISIS particle array in coincidence with the GASP germanium array [12]. These methods are based on the detection of both α-particles in the same detection cell using the peculiar response function of the "pile-up" event firstly observed by Wozniak et al [11] in order to identify particles. The "pile-up" methods obviously suffer for the background due to random coincidences that must be correctly evaluated.

Since more than 20 years we are using the CHIMERA detector [15, 16] at LNS INFN laboratory in Catania and more recently we coupled with it an ancillary detector with improved granularity and angular resolution, the FARCOS array [17–20]. Each telescope

of the FARCOS correlator is made of three detection stages. The first two are DSSSD (Double Sided Silicon Strip Detectors), made of 32 horizontal strips in the front side and 32 vertical strip in the back one allowing a very good angular resolution measurement of the detected particles; we will show the advantage of this in the energy resolution of the ^{8}Be measurement. Given the different detection techniques used and the peculiarity of these two particles arrays we have collected sufficient data to make an extensive study on ^{8}Be identification. In particular, we will discuss some identification methods based on pulse shape analysis never published in the literature. We will shortly discuss the different methods comparing their use. Moreover we will also show with detailed Monte-Carlo simulations some procedures that can be used to improve the precision of the measurement using pile up methods. We underline that the methods here presented can be relatively simply extended to the measurement of resonances of light medium nuclei with special attention to resonances in exotic nuclei at the border of drip lines, that have a high relevance in present studies of modern nuclear physics. In fact, generally, these nuclei are studied in inverse reaction kinematics, therefore the decay cone of particles is rather narrow in the forward direction, due to the strong kinematic boost of the beam linear momentum. Consequently, both kinematic and "pile-up" identification methods can be used for the detection of such resonances.

2 Kinematic methods

As discussed in the introduction, kinematic identification methods for the ^{8}Be detection are used since long time in nuclear physics [4]. The small energy of the resonance usually produces a narrow decay cone of the two α-particles allowing the arrangement of two or more detectors needed to reconstruct the decaying particle. The measure of this resonance with a reasonable energy resolution is generally straightforward.

Figure 1 shows (red histogram) ^{8}Be excitation energy spectrum, observed by measuring in coincidence two α-particles in the angular region between 30°–50°, angles covered by the sphere of the CHIMERA detector. In this angular region, the opening angle of the detectors is $\theta = 8°$ (polar angle) and $\phi = 11.5°$ (azimuthal angle). This spectrum was detected in the reaction $\alpha + {}^{12}C$ measured at 64 MeV beam energy for the study of the decay of excited ^{12}C levels [22]. The resonance of the ^{8}Be$_{G.S.}$ with the peak around 100 keV can be well seen; furthermore, also the first excited state at around 3 MeV is observed. The position of the peaks is not exactly what expected mostly due to the error performed in the detection angle of the particles but also due to the effect of spurious coincidences (yellow spectrum normalized to reproduce the high energy background). The energy resolution, as it is estimated in ^{8}Be$_{G.S.}$ peak, is of the order of 50 keV. Evidently due to the small value of the resonance peak, the relative error is quite large, more than 50%. The large relative error depends mainly on the angular resolution of the used detectors. A fundamental ingredient for the reconstruction of the relative energy of the two particles is in fact the correct measurement of the detection angle. At least two choices can be performed with large size detection cell. The first one is to use the centroid of the detector (CA in the following). This choice is used for the red histogram, shown in Fig. 1. The second one is to use a random angle (RA) chosen in the angular range covered by the detector cell. When applied to the same set of raw data, this last choice produces the filled cyan histogram of Fig. 1 with a larger relative energy resolution, around 70 keV. Therefore, using the CA choice we have a better resolution, as shown in Ref. [14]. This is due to the smaller average difference between the real detection angle and the assigned one, as we will show in the simulation paragraph. However, in some cases, the fixed angular difference of the detection angles can generate spurious structures. One of these structures can be noticed for instance in the red spectrum between 200 and 400 keV, while a more smooth behaviour is seen with the RA choice. Anyway, when spurious fluctuations appear closer to a peak of physical interest or with low statistics, the RA choice is better [21].

To understand the effect of the angular resolution on the shape of the ^{8}Be$_{G.S.}$ resonance, in Fig. 2 we show this peak as extracted by analysing α-particles coincidences (CA choice, normalized to the maximum) collected in two other rings of the CHIMERA detector, namely ring 8I and ring 9E, centered respectively at 21° and 28.5°. The Gaussian parameter σ, extracted from the fit of the peak, is reduced to only 18 keV for the ring 9E (filled cyan spectrum $\Delta\theta = \pm 1.5°$), with respect to the more than 50 keV of the sphere. It is further reduced to 14 keV for ring 8I (filled yellow spectrum $\Delta\theta = \pm 1°$).

Fig. 1 ^{8}Be excitation energy spectra observed measuring in coincidence two α-particles in detectors of the spherical region of CHIMERA. The filled cyan and empty red spectra are evaluated respectively with the RA and CA assumptions on the detection angle of α-particles (see text), the ground and first excited states can be observed. The yellow spectrum is the background evaluated with the mixed event method [21]
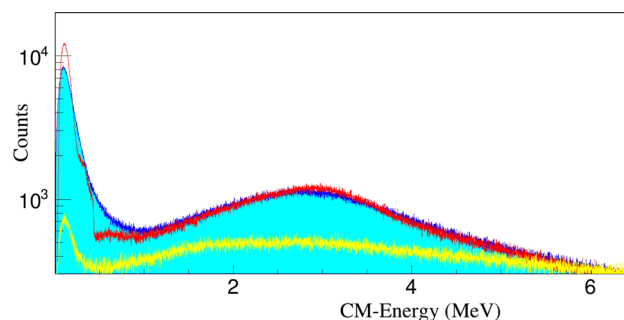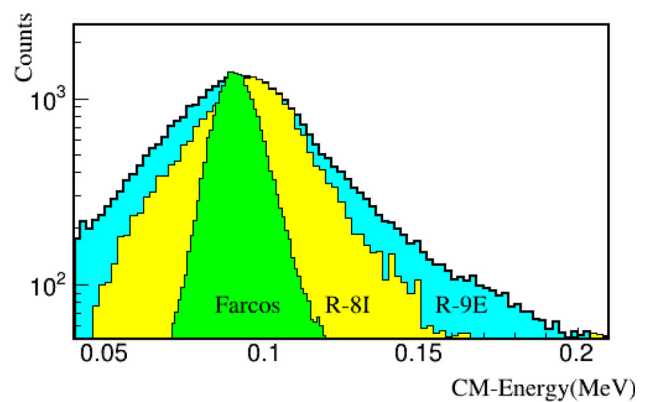
Fig. 2 Comparison of the $^8Be_{G.S.}$ energy width, detected in different rings of CHIMERA and with FARCOS detectors. The different width observed is a consequence of the angular resolution of the detectors

In the same plot, we also show the peak measured in the same reaction with the new FARCOS array (filled green spectrum). In this case we measure a σ value of the peak of about 7 keV. This is due to a much better angular resolution obtained with the 2 mm wide front and back strips of the first two stages, providing a precision $\Delta\theta = \pm 0.14°$ when mounted at around 40 cm of distance from the target. The thickness of the silicon strip detectors (300 and 1500 µm) is enough to stop α-particles with energy up to 65 MeV. Thus, they can be easily detected and identified, with an energy resolution which is better than the ones obtained with the telescopes of CHIMERA, where the second stage is a CsI(Tl) scintillator. The quite good absolute error of 7 keV can be obtained only with a precise measurement of the angle of each pixel of the detector. In the case of FARCOS detector, this is performed by using a laser system as described in Refs. [17, 23].

3 "Pile-up" methods

In the previous paragraph we have observed the disadvantage of using large detectors in the reconstruction of the excitation energy by kinematics. However, large surface detectors provide an opportunity for the application of the "Pile-up" methods. We specify that in these methods both α-particles are detected in the same detector and one can use the information given by that only detector to identify the ^8Be. In effect, CHIMERA telescopes of the spherical region benefit from a relatively efficient detection mode with "Pile-up" methods. Many identification techniques are used with CHIMERA detector, as shown recently in [16], and in all these methods we can observe the particular response function of ^8Be events. In the following, we will start discussing the most peculiar method used by CHIMERA i.e. the Time of flight method (TOF). In successive paragraphs we will present the "pile-up" effects in silicon and CsI(Tl) pulse shape methods and finally we will close with the well known ΔE-E method.

3.1 ^8Be identification by Time of flight technique

This identification method is the most peculiar for the CHIMERA detector design [24–27] and it mainly decreases as much as possible the energy threshold for particle identification. For example, thanks to the use of Time-of-flight (TOF) technique it is possible the identification of target-like fragments with mass around $A = 20 - 30$ in semi-peripheral reactions and velocity thresholds as low as 0.5 cm/ns or less [28].

In this case, it is quite simple to show that ^8Be events behave effectively as a particle of mass $A = 8$ stopped in the detector. For the sake of simplicity, we can assume that the 2 particles have the same energy, written as function of the velocity V_α, in the non relativistic approximation (reasonably good for particles stopped in the 300 µm silicon detectors of CHIMERA) $E_\alpha = 1/2 m_\alpha V_\alpha^2$. It is clear that summing two equal energy α-particles, the energy is equivalent to the one of a particle with the same velocity and two times the mass of the particle, namely mass 8.

A scatter plot with energy and time of flight (TOF) of particles detected in the silicon detector of the CHIMERA sphere, in the reaction $\alpha+^{12}C$ at 64 MeV, is shown in Fig. 3. The three lines plotted in such plot show the expected non relativistic correlation between energy and time for masses 4, 8 and 12. One can note that the lines follow the observed trend of the events at least at low energy. Some distortion is observed at higher energy (increasing with the charge of the particle) due to differences in the signal rise time that slightly changes the response function of the CFD discriminators (as better discussed later). One has to note that the largest effect of the signal rise time is observed for higher energy particles, that are stopped in the low field region of the detectors, where the charge collection is slower. As it will be shown in the simulation section, the energy of the two α-particles from the decay of ^8Be stopped in the same detector is generally not equal and in the case of the studied reaction it can have a difference of the order of 2–3 MeV. This difference in the energy of the two particles produces a small time difference in the arrival of particles on the detector, that in detection systems equipped with digital acquisition of adequate frequency could be used to discriminate the "pile-up" events from single particle detection. In the used analogic ACQ these signals are integrated with 1 µs shaping time and

Fig. 3 Energy and time of flight scatter plot of particles detected in the reaction $\alpha + {}^{12}C$ at 64 MeV. The behaviours expected for particles of mass 4, 8 and 12 are plotted as lines
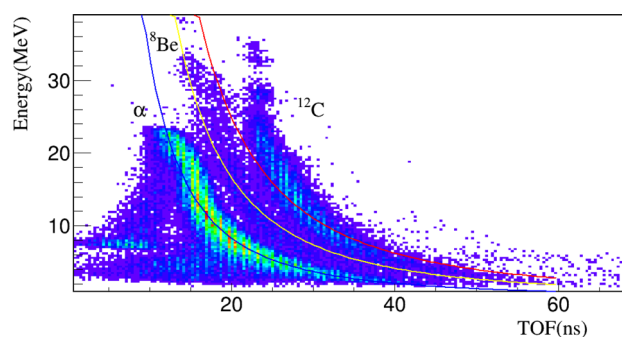
do not produce significant variation in the energy sum of the two particles, while the time of the faster particle generally dominates the time response of the discriminator. To well reproduce this behaviour, we did a simple simulation of the event, where the spread observed on the $T^2 = md^2/(2 \cdot E)$ line (being m the particle mass and d the travel distance) is within the energy (E) and time (T) resolutions of our detectors.

3.2 ${}^8Be$ identification by pulse shape analysis on silicon detectors

Continuing to discuss the identification of particles stopped in a silicon detector, it is well known that the plasma produced inside a silicon detector by the interacting ions can strongly perturb the electric field inside the detector, changing the collection time of electrons and holes [25]. This effect, somewhat presented in Fig. 3, was studied since long time [29, 30] and it is now used in various detection systems in order to identify in charge and sometime also in mass, particles stopped inside silicon detectors [30–34]. This effect is particularly enhanced when the particles impinge on the low field side of the detector. However, it is also present when, as in the case of the CHIMERA detectors, the particles experience a high electric field in the initial portion of their track in the detector (front injection), thus producing a faster signal for time measurement [35]. We exploit, since many years, this effect with a dedicated electronics based on the measurement of the signal rise time. The method used is based on the availability of two CFD channels with different fractions, where the first one with 30% fraction, measures the starting time of the signal, the second CFD is set with a 80% fraction, and it approximately measures the time when the signal reaches the 80% of its maximum. The time difference between the two CFDs is proportional to the signal risetime. The electronics is implemented with N1568b 16 channel CAEN modules in which, for each channel, a spectroscopic and a time amplifier are present, plus a stretcher for the energy signal and the two CFD with automatic walk adjustment for the time and risetime measurement. An example of the obtained charge identification is shown in Fig. 4. In this figure we plot the energy and rise time of particles detected in the reaction ${}^{78}Kr + {}^{40}Ca$ at 10 AMeV [36, 37]. A nice identification of ions up to charge at least 8 is shown by this detector of the CHIMERA sphere, placed at 34° (the dynamic is small in such a reaction, at relatively large angles, due to the inverse kinematics). Also mass identification can be observed for Beryllium isotopes, enhanced by the missing ${}^8Be$ events. We will find the place where these missing events actually produce a signal. To our knowledge the possibility to identify ${}^8Be$ also with pulse shape "pile-up" method was never been explored until now. We will show with an example that such events can be observed near the Lithium region. If the energy of the two α-particles is not so much different and their arrival time in the detector is simultaneous within the detector time response, the two pulses can be simply summed. Assuming that a step signal is generated in the preamplifier, with a defined rise time, the two signals will reach the maximum in approximately the same time. Thus, a good approximation is that the ${}^8Be$ signal has the same rise time of the single α-particle but with a corresponding doubled energy. Using the identification line observed for α-particles and multiplying by a factor 2 its energy, we can therefore generate the region expected for 2-α "pile-up" events.

This is done in the lower inset of Fig. 4 (red dots). The region is placed roughly between Lithium and Beryllium ions. Once defined the region where ${}^8Be$ events are expected we can rather well identify them both in the main picture or in the upper inset where the zoomed view is plotted. The smaller dynamical range of these 2-α event with respect to the one of the ${}^{7,9}Be$ events is due to the larger range in silicon of α-particles, thus the particles with larger energies punch-through the silicon detectors and can not be observed in the RT-Energy plot of Fig. 4. One can also note that the slope of the line identified as ${}^8Be$ is also slightly different with respect to the nearest Li lines. The distance of this line from the ${}^{6,7}Li$ lines is similar to the distance from the ${}^{7,9}Be$ lines, so the ${}^8Be$ region seems the one where ${}^9Li$ should be observed. For neutron-poor reactions this simplifies the identification, being the expected ${}^9Li$ contamination rather small. The TOF technique, discriminating among different masses, could be used to clean from this possible background, but in our case with only 40 cm of time-flight path, the time resolution is not sufficient for this goal.

The 2-α line here observed was deduced assuming α-particles of equal energy. In the more usual case of two α-particles with different energy (see Sect. 4) the measured rise time can be affected by the different time of flight of the two particles. Due to the small flight path (only 40 cm) this change is of the order of few ns. This is inside our error bars as can be easily estimated from the plot.

Fig. 4 Energy and rise time scatter plot of particles detected in the reaction $^{78}Kr + ^{40}Ca$ at 10 AMeV. The particles detected with different charge Z can be observed. In the lower inset a zoom around the Lithium region is shown. Red dots are obtained multiplying by a factor 2 the energy of α-particles, this is the region where ^8Be is expected. In the upper inset the presence of ^8Be events in such region can be better noted
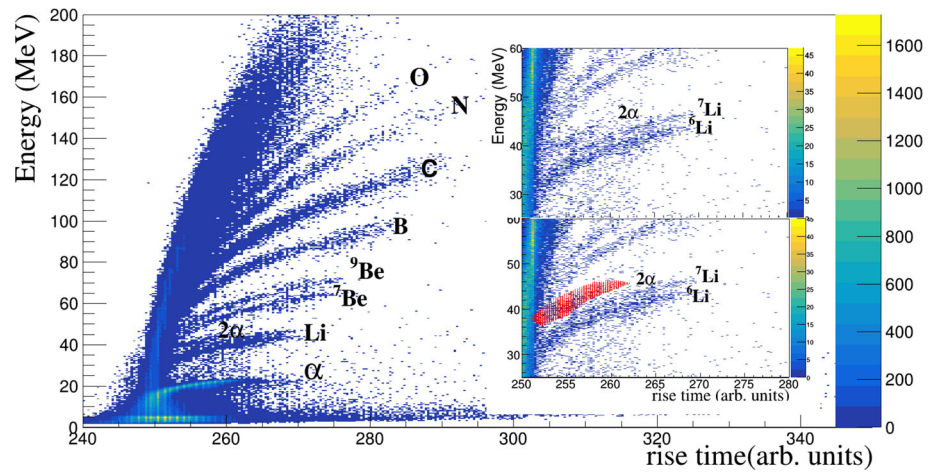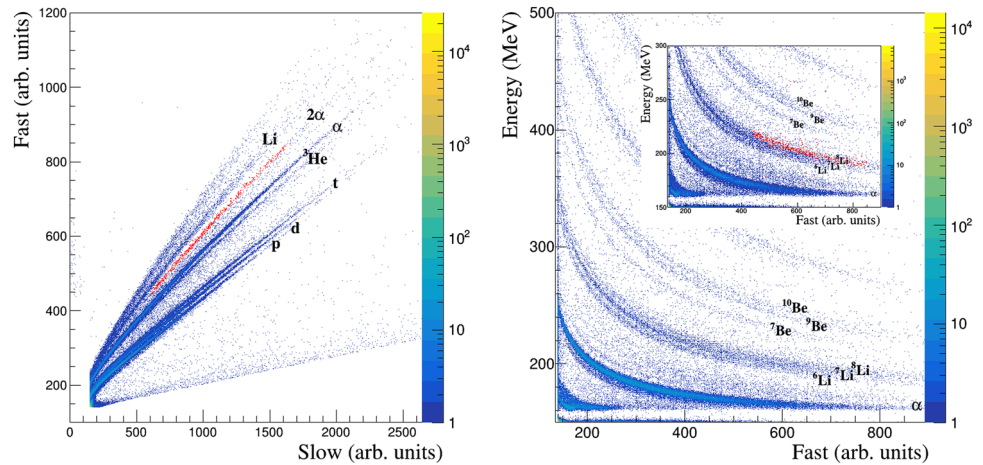

Fig. 5 a Fast-Slow correlation plot for the reaction $^{124}Xe+^{64}Ni$ at $34°$. **b** ΔE-E scatter plot for the same detector, in the inset a zoom around the zone of Lithium lines is plotted. The red dots are the events that in the Fast-Slow plot are labelled as 2-α

3.3 ^8Be identification by pulse shape analysis on CsI(Tl) detectors

The light produced by the particle interaction with CsI detectors (Tl doped) is strongly dependent on the charge and mass of the impinging ions. Therefore, we can use such peculiarity to perform particle isotopic identification. Various identification techniques were developed for the CsI(Tl) detectors, see for instance [16, 18]. For CsI(Tl) of CHIMERA detector we use the two gate method described in Ref. [38]. As well illustrated in [39], two different scintillation modes are present in the CsI(Tl) detectors. They have a different sensitivity to the charge of the detected ion and are also characterized by different decay times. In our case the Slow signal is particularly enhanced when low ionizing radiations are detected as electrons, γ rays and ultra relativistic particles. The Slow contribution instead decreases when more ionizing particles as proton, deuteron, triton, α-particles and so on are detected. A saturation of the discriminating power of the scintillator is obtained for charges 4–5 depending on the crystal quality. The Fast signal is proportional to the energy released by the particle. This signal is also smoothly depending on the ionizing power of the particle. This produces a small quenching effect in the response function of the detector, as a function of the detected charge, well described by the Horn formula [40, 41]. When two α-particles of similar energy are detected in the scintillator, we measure the sum of the two Fast component. Also the Slow signal is the sum of their two Slow signals. This means that the ratio Fast/Slow should remain constant. This is different however from the behaviour of a single α-particle of double energy. In fact, increasing the energy of the α-particle, its ionizing power decreases, consequently the Slow component contribution increases, and the observed ratio Fast/Slow is slightly smaller. This is the reason why the two-α events generate a line in the Fast-Slow plot different from the one of α-particles, namely a region from ^6He and ^6Li near the region where ^8He should be found [42]. In most reactions the production of ^8He is so small that can be neglected and all events attributed to ^8Be. In Fig. 5a an example of this behaviour is shown. Fast-Slow components plot for a telescope of the ring 10 in the reaction $^{124}Xe+^{64}Ni$ at 35 AMeV are shown where the $^8He/2$-α line is quite evident (red dots). The proof that these events are really 2-α events detected in "pile-up" in the same detector, coming from the decay of a ^8Be nucleus, is given by the fact that the particles in the line labelled as 2-α lie on the ^8Li line in the ΔE-E matrix in Fig. 5b), as we can observe in the inset, where they are also reported as red dots. As we will show in the next paragraph this behaviour, in our telescopes, is the signature of 2-α produced in the decay of a ^8Be nucleus.

3.4 ^{8}Be identification by ΔE-E analysis

This identification method works rather well when both α-particles have enough energy to pass the first stage of telescopes. As told in the introduction, this method was used since long time [11] and it is particularly useful in particle-γ coincidence experiments as a tagging method to select definite reaction channels, as done in [12]. In this case, the 2-α event generally does not behave as a Beryllium ion, as already observed in the silicon pulse shape method. And in fact, the missing ^{8}Be line in the ΔE-E scatter plot is an important signature, often used as a reference point to identify the charge and mass of the observed lines in such plots (see Figs. 5b, 6). The 2-α behaviour can be understood analytically by using the approximate dependence of the energy loss signal from the energy, mass and charge of the particle as shown in [11]. Assuming K constant (depending on the detector properties) and being A and Z respectively the mass and charge number of the particle, approximately we can write: $\Delta E = K \cdot A \cdot Z^2 / E$. For a ^{8}Be event with 2 α-particles detected in the same detector, if the energy of the two α-particles is approximately equal, we can write $\Delta E_{8Be} = 2 \cdot \Delta E_\alpha = 2 \cdot K \cdot A_\alpha \cdot Z_\alpha^2 / E_\alpha$. Taking into account that $E_\alpha = 1/2 \cdot E_{8Be}$ and inserting mass and charge of α-particles we have $\Delta E_{8Be} = K \cdot 64 / E_{8Be}$. Therefore, the $A * Z^2$ constant becomes 64. This value is very close to 63 that is the value expected for ^{7}Li events. Obviously the 2α loci can be mixed with ^{7}Li ones, in fact this isotope is in general abundantly produced in Heavy Ions reactions. In order to better observe 2-α events, one can screen the detectors from ^{7}Li with absorbers as was done in [12], or alternatively, ^{8}Be particles can be selected by using a double identification method combining the ΔE-E analysis with the pulse shape analysis of CsI(Tl) signals, as shown in the previous paragraph. The peculiar behaviour of events with ^{8}He characteristics in the Fast-Slow CsI(Tl) line and with Lithium properties in the ΔE-E plot makes this method relatively robust. In the case of CHIMERA detectors, as already shown in Fig. 5b), however we do not observe the two "pile-up" α-particles as ^{7}Li in the ΔE-E plot, but they are observed as ^{8}Li. In fact, because of the above described quenching effect on the scintillator light production, the energy response function of CsI(Tl) detectors decreases by increasing the charge of the nucleus. Therefore, the energy of 2 α-particles produces more light than an equal energy of a ^{7}Li ion; as a consequence events are moved around the line corresponding to ^{8}Li ions. This has the advantage to further reduce the background for the ^{8}Be identification because ^{8}Li is surely produced with smaller probability than ^{7}Li in most reactions between stable nuclei.

Another effect that certifies the identification of such events as 2 α-particles detected in "pile-up" can be noted by comparing ΔE-E plots of ring 8E, Fig. 6a, (angular coverage $23° \pm 1°$), and ring 10, Fig. 6b, (angular coverage $34° \pm 4°$). The plot is relative to the reaction ^{78}Kr+^{40}Ca at 10 AMeV beam energy [43]. This reaction is between neutron poor ions, thus we do not expect to populate neutron rich isotopes [36]. This is evident also by the large population of ^{6}Li with respect to ^{7}Li and ^{7}Be with respect to ^{9}Be. However in both spectra, (more evidenced in Fig. 6b) we note events in the region of ^{8}Li, with a clearly different energy loss dynamical range behaviour. The residual energy of these events is larger than the residual energy of the other lithium ions. This is again another signature of the fact that we are looking two particle "pile-up" events combined with the smaller quenching of α-particles with respect to lithium ions. The larger solid angle of the ring 10 detector increases the detection efficiency of ^{8}Be events, with the effect of apparently enhancing the detection yield of ^{8}Li ions.

Finally we should note in Fig. 6b the presence of other "pile-up" events. A group of events can be envisaged in the region near ^{6}He where we are probably observing p+α "pile-up". Moreover 2p events seem also present as it can be noted by looking to the forth line in the region of Z=1 isotopes.

4 ^{8}Be simulations

If a ^{8}Be is detected and identified by one of the above described "pile-up" methods, the event can be treated in the analysis as a single particle fully identified in charge, mass and total energy. However, as we will show in the following it is not obvious that two α-particles measured in the same detector always come from a decaying ^{8}Be. Consequently, in this last case, it is necessary to consider anyway the detected event as two separate α-particles (for instance in order to extract the correct reaction Q-value) assigning the appropriate energy and detection angle to each of them. As done in the previous paragraphs, one could simply estimate that the energy of each particle is one half of the total detected energy. This is reasonably good, as a first approximation, for experiments realized by using high energy beams, while it can be wrong in the case of low energy experiments. In fact, to be measured in the same detector, thus in the same approximate direction, the α-particles must be emitted in two opposite sides with respect the original ^{8}Be velocity vector. In this case, at low energy, the sum of the speed of the Center of Mass (^{8}Be) and of the decay speed can be quite different producing a not negligible variation in the energy of each particle. As above outlined, for instance in the case of ^{12}C decay, it is not obvious that the two α-particles detected together belong to a ^{8}Be decay. In this paragraph we will present results of simulations performed for a low energy reaction α+^{12}C at 64 MeV beam energy, showing examples of all these effects. Simulations will be performed for the CHIMERA detector following the recipe of Ref. [21] . We will concentrate our attention on the study of the recoiling excited ^{12}C emitted from 30° to 60°, the region with the highest efficiency for "pile-up" methods for the CHIMERA detector.

In this angular region the ^{12}C has a relatively low energy, lower than 30 MeV, depending on the detection angle and excitation energy of the level. Looking for instance to the decay of the Hoyle state of the ^{12}C, performed simulations show that in about 20% of the cases two α-particles can be observed in the same silicon detector. However, in more than 44% of these cases the two α-particles

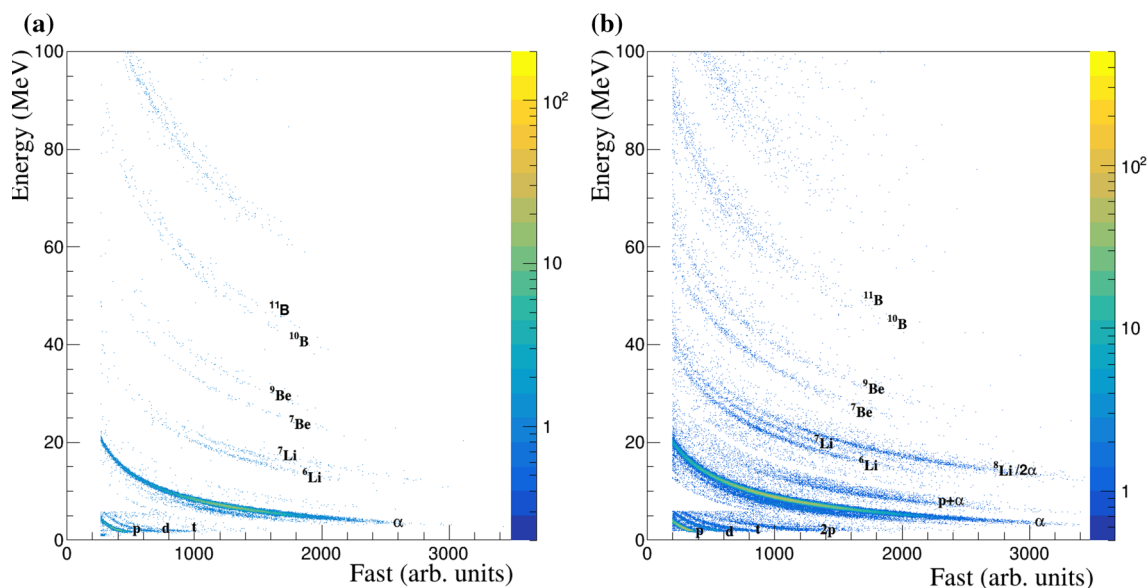**Fig. 6** ΔE-E correlation plots detected in the reaction $^{78}Kr +^{40} Ca$ at 10 AMeV at **a** 23° ring 8E and **b** 34° ring 10. In the plot **b** the larger solid angle covered by the detector produces a higher contribution of "pile-up" events 2p, 1p+1α, and 2α-particles detected in the region of ^{8}Li with much larger energy with respect to other lithium isotopes

Fig. 7 Simulated correlation plots between the laboratory energy of two α-particles measured in the same detector in the reaction $\alpha +^{12} C$ at 64 MeV beam energy. The α-particle decays of the Hoyle state in $\alpha+^8$Be is assumed. **a** The two particles are emitted in the decay of the ^{8}Be. **b** The two particles are the first emitted α-particle and one of the other two α-particles from the ^{8}Be decay
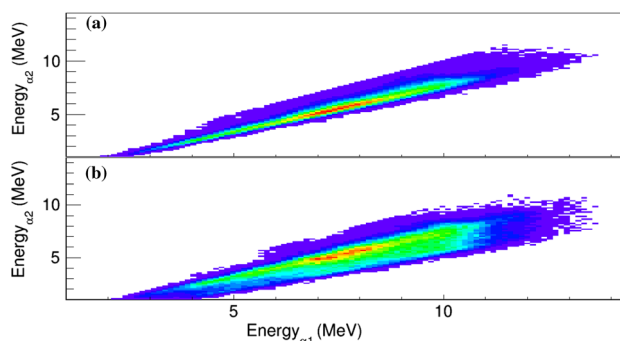

do not belong to a ^{8}Be decay. In fact, one α-particle has origin from the first α-decay of the ^{12}C and the other one α-particle from the sequential decay of ^{8}Be residue. As shown in Fig. 7a, b, the sharing of energy between the two particles is different in the two cases. In the top panel the energy sharing of the two α-particles is shown in the case they belong really to the ^{8}Be decay. In the bottom panel the other case is shown. The energy sharing of the two α-particles belonging to ^{8}Be is rather well defined by the reaction kinematic. The particles were ordered to have the energy of α_1 larger than the energy of α_2. This means that α_1 was emitted in the same direction of the original ^{8}Be and thus with larger energy in the laboratory reference frame. The energy difference between the two particles can be of the order of 3 MeV or more. Even larger fluctuations in the energy distribution are observed when the two α-particles do not belong to a real ^{8}Be (see Fig. 7b) . This depends on the fact that their emission angles in the CM system are not correlated. In this case the energy difference is larger due to the larger CM energy of the two particles (see Refs. [21, 44]).

4.1 The best ^{8}Be method

As discussed in the introduction, we can use simulations to compare the ability of different analysis methods to attribute a correct energy and detection angle to each of the two α-particles detected in pile-up. The most simple method is to share the energy between the two α-particles requiring that they are really due to a ^{8}Be decay, therefore their CM energy must be 92 keV. We have shown that this is not always true, and it is therefore interesting to observe the effect of such an assumption. We call this method "best ^{8}Be". A search loop can be defined in the data analysis program, sharing in a random way the energy between the two α-particles and by assigning them a random angle inside the area covered by the detector (in this case the CA approximation is clearly not useful). The CM energy of the two particles can be evaluated with a vector algebra, for instance with the Root TVector3 class, being negligible relativistic corrections. Once calculated, this CM energy can be compared to the 92 keV assumed within a window of the energy resolution. If the computed energy is out of this window the calculation can be repeated for a defined number of iterations. Over these iterations one can assume that this is not a ^{8}Be event and reject it.

Fig. 8 CM excitation energy of the Hoyle state computed assigning energy and angle of the particles with "best ^{8}Be" and "BRE" methods. The filled red histogram is obtained with "best ^{8}Be" for true ^{8}Be events measured in one detector. The filled yellow histogram is obtained for two α-particles not belonging to ^{8}Be. The cyan histogram is the sum of the two contributions. The green histogram is obtained minimizing the energy of the Hoyle resonance with BRE method. In the inset the dots are the average number of iterations needed to minimize data with "BRE" method searching for a resonance as a function of its energy
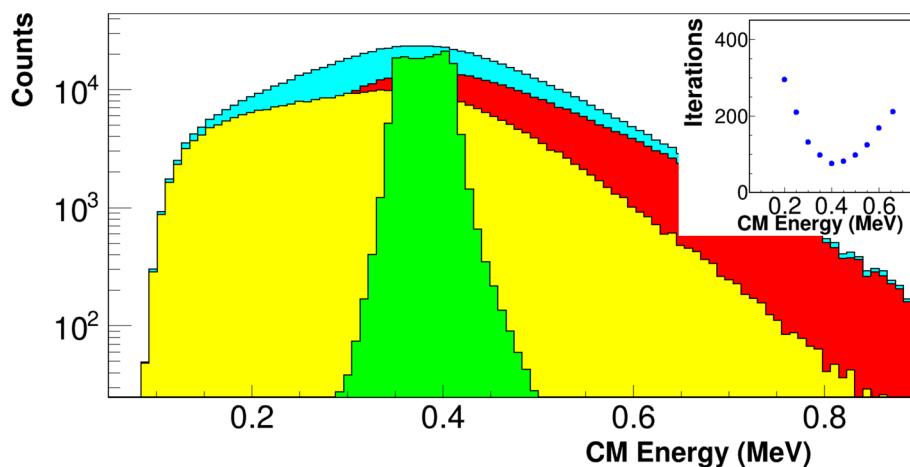
As outlined the limit of this method is that it often fails to reasonably account for events not belonging to a real ^{8}Be. Therefore the reconstruction of the excitation energy of the Hoyle state can be worse as shown in Fig. 8. In fact, in this figure we note a smaller average CM excitation energy with respect to the 380 keV available for the Hoyle state reconstructed with this method for events with α-particles measured in the same detector not belonging to ^{8}Be (yellow filled spectrum). While a more symmetric distribution is obtained for true ^{8}Be events (filled red histogram).

The filled cyan spectrum is the sum of the two contributions. The suggested method cannot therefore improve the global total energy resolution of the measurement because the random angle chosen optimizing only the CM energy of the ^{8}Be particle can deteriorate the total CM energy for instance of 3-α events.

4.2 The Best Resonance Energy method

A more constrained method could be used for events with one α-particle in coincidence with two "pile-up"-α-particles, trying to fulfil the whole characteristics of the 3-α resonance from which these particles were produced. We call this method best resonance energy (BRE). In Fig. 8 an example of the use of this method is plotted as filled green histogram. We note that with BRE we can obtain a much better energy resolution than with the use of the simple CA, RA or best ^{8}Be methods. This is because we choose the random angles assigned to all the three detected α-particles and share the energy of the two α-particles observed in the same detector, requiring that the CM energy of the 3-α-particles system corresponds to the one of the Hoyle state. This is done within a defined energy window that after we can identify as the width of the peak. Obviously we also require that one of the three pairs of α-particles comes from the decay of a ^{8}Be (assuming to be negligible the direct 3-α decay probability [45]). Adopting a reasonable error bar (± 30 keV in the plotted example) for the correspondence with the Hoyle resonance energy (± 10 keV for the ^{8}Be) and by optimizing the search strategy one can find a solution for each event on average with around 70 iterations. We note however that the peak has a not Gaussian shape. This is just one of the characteristics showing that the obtained resolution is artificially small. In fact, for each event there are many possible solutions and the chosen one is not necessarily the correct one. We could search if the same events belong to a status with a different excitation energy, finding also a solution. However, we must note that if in the simulated data coming from the decay of the Hoyle state we search solutions for a different resonance energy, much more iterations are required on average in order to obtain the correct angle and energy partition of the detected α-particles. This required average number of iterations needed as a function of the resonance energy assumed is plotted as dots in the inset of Fig. 8. The minimum is observed at around the correct energy of the Hoyle resonance. This method could be adopted searching for an unknown resonance energy. The width of this distribution gives a more realistic value of the resolution that could be attained with this method (approximately 200 keV FWHM). Also the ^{8}Be spectrum is improved when the BRE method is used. In Fig. 9 we can compare the ^{8}Be CM energy spectrum obtained with the best ^{8}Be method (red empty histogram) with the one extracted with the BRE (filled cyan histogram). In both cases a ± 10 keV energy window was selected to get the correct ^{8}Be resonance energy. The strong request to consider any 2-α pair as a ^{8}Be produces a not symmetric peak in the best ^{8}Be method. Some little improvement on the shape of the peak is obtained in the BRE case. However the limitation on the detection angular range of the two α-particles stopped inside a detector does not allow to produce a reasonably symmetric peak. In the inset it is shown an application of the BRE method to 3-α events collected in 3 different detectors. Two cuts in the energy window are shown, ± 10 keV (filled green histogram) and ± 30 keV (empty blue

Fig. 9 ^{8}Be center of mass energy spectra obtained in the case of best ^{8}Be method (red empty histogram) and BRE (filled cian hystogram). While in the inset the same spectrum is shown in the case of 3α-particles detected into 3 different detectors applying the BRE method with ± 10 (green filled histogram) and ± 30 keV (blue empty histogram) precision window
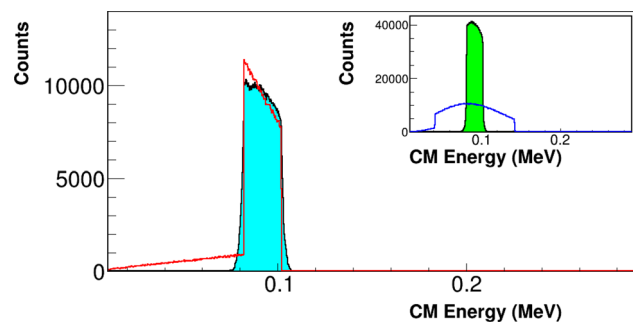

Fig. 10 Difference from the true angle and the one assigned by different data analysis methods in the simulated Hoyle state decay in the reaction $\alpha + ^{12}$C at 64 MeV, with particles detected in the CHIMERA sphere. The filled yellow histogram is the CA choice; the filled cyan spectrum is the RA choice; the empty red histogram is obtained assigning the best angle in the search of the Hoyle resonance (see text)
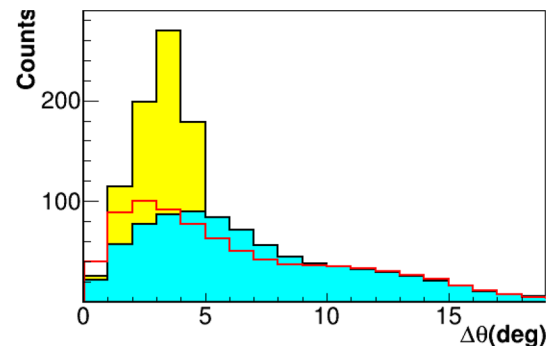
histogram). A more symmetric behaviour of the peak can be observed and in the case of ± 30 keV window a Gaussian fit can be performed producing a σ value of about 45 keV. Due to the error in the angle the peak it is not exactly centred around 92 keV.

Analysing simulated data it is simple to characterize the quality of the analysis procedures in order to compare the different methods. We can for instance measure the difference between the angle resulting from the minimization procedure and the real one (obtained by the Montecarlo procedure, in the simulation of the event). We note that the BRE method (empty red spectrum of Fig. 10) produces, in more events than with the other methods, a result that is less than one degree different from the real angle. Moreover the maximum of its distribution is peaked at 2.5° therefore it is better than the one of CA (yellow filled spectrum with maximum at 3.5°) and RA distribution (cyan filled spectrum with maximum at 4.5°). However, the σ of the distribution of the CA method is narrower, while a large tail of the distribution is present for the BRE method, rather similar to the RA choice. This method is therefore surely better than RA distribution, but generally the CA choice is still the best one comparing the three different methods.

5 Conclusions and outlooks

In this paper we have presented and analysed the various methods available with the CHIMERA+FARCOS arrays for the identification of ^{8}Be events. The availability of many identification methods, that can be also applied in combination, allows a clean extraction of events with a large background reduction. Some of the used methods have a response function depending on the peculiarity of our detector as shown in the paragraph relative to the ΔE-E analysis. However, in general the described methods can be extended to many other kind of detection systems. The crucial importance of the angular resolution of the measurement in order to obtain an accurate energy of the observed resonance was also pointed out. In the last section, the evaluation of the energy sharing between two α-particles impinging on the same detector is investigated. More in detail, we analysed the possibility to extract from the experimental data, the information about the energy of each α-particle emitted in "pile-up" events, by imposing external constraints as the reproduction of ^{8}Be$_{G.S.}$ peak or of resonances as the Hoyle level. We have evidenced that, apart from spurious coincidences, it is not always true that two α-particles impinging in the same detector belong to a ^{8}Be, especially in reactions involving light medium nuclei with strong α-cluster structures and high α-particle multiplicity, like ^{12}C, ^{16}O, or ^{20}Ne and others. The precise understanding of these detection methods is crucial for their extension to the study of resonances in light nuclei near to drip lines, that are important for the investigations of reactions with exotic beams.

References

1. D. Tilley, J. Kelley, J. Godwin, D. Millener, J. Purcell, C. Sheu, H. Weller, Energy levels of light nuclei A=8,9,10. Nucl. Phys. A **745**(3), 155–362 (2004). https://doi.org/10.1016/j.nuclphysa.2004.09.059
2. F. Hoyle, On nuclear reactions occuring in very hot stars. I. the synthesis of elements from carbon to nickel. Astrophys. J. Suppl. Ser. **1**, 121 (1954). https://doi.org/10.1086/190005
3. M. Freer, H. Fynbo, The Hoyle state in ^{12}C. Prog. Part. Nucl. Phys. **78**, 1–23 (2014). https://doi.org/10.1016/j.ppnp.2014.06.001
4. J. Cramer, K. Eberhard, N. Fletcher, E. Mathiak, H. Rossner, A. Weidinger, An array detector for the spectroscopic study of reactions producing ^{8}Be and ^{8}Be*. Nucl. Inst. Methods **111**(3), 425–430 (1973). https://doi.org/10.1016/0029-554X(73)90197-3
5. T. Sugimitsu, N. Hori, A ^{8}Be detection system for angular distribution measurements. Nucl. Instrum. Methods Phys. Res., Sect. A **309**(1), 218–221 (1991). https://doi.org/10.1016/0168-9002(91)90105-Y
6. K. Ideno, Y. Tomita, Y. Sugiyama, H. Ikezoe, S. Hanashima, Y. Nagame, A two-dimensional position-sensitive detection system for the ^{8}Be nuclei in heavy ion reactions. Nucl. Instrum. Methods Phys. Res., Sect. A **302**(2), 385–387 (1991). https://doi.org/10.1016/0168-9002(91)90428-S
7. E. Macdonald et al., A high efficiency ^{8}Be detector. Nucl. Instrum. Methods Phys. Res., Sect. A **317**(3), 498–505 (1992). https://doi.org/10.1016/0168-9002(92)90993-E
8. S. Allcock, P. Keeling, W. Rae, A. Smith, S. Bennett, M. Freer, B. Fulton, R. Page, P. Woods, A compact high-efficiency ^{8}Be detector. Nucl. Instrum. Methods Phys. Res., Sect. A **289**(1), 213–220 (1990). https://doi.org/10.1016/0168-9002(90)90261-4
9. D. Artemenkov, V. Bradnova, M.M. Chernyavsky et al., Unstable states in dissociation of relativistic nuclei. Eur. Phys. J. A **56**, 250 (2020). https://doi.org/10.1140/epja/s10050-020-00252-3
10. A. Zaitsev, D. Artemenkov, V. Glagolev, M. Chernyavsky, N. Peresadko, V. Rusakova, P. Zarubin, Correlation in formation of ^{8}Be nuclei and α-particles in fragmentation of relativistic nuclei. Phys. Lett. B **820**, 136460 (2021). https://doi.org/10.1016/j.physletb.2021.136460
11. G.J. Wozniak, H.L. Harney, K.H. Wilcox, J. Cerny, α-particle transfer via the $(^{12}C, ^{8}Be)$ reaction: Application to studies of ^{16}O and ^{20}Ne. Phys. Rev. Lett. **28**, 1278–1281 (1972). https://doi.org/10.1103/PhysRevLett.28.1278
12. S. Thummerer, W. von Oertzen, B. Gebauer, S.M. Lenzi, A. Gadea, D.R. Napoli, C. Beck, M. Rousseau, The population of deformed bands in ^{48}Cr by emission of ^{8}Be from the ^{32}S+^{24}Mg reaction. J. Phys. G: Nucl. Part. Phys. **27**(7), 1405–1420 (2001). https://doi.org/10.1088/0954-3899/27/7/303
13. J. Bishop, T. Kokalova, M. Freer et al., Experimental investigation of α condensation in light nuclei. Phys. Rev. C **100**, 034320 (2019). https://doi.org/10.1103/PhysRevC.100.034320
14. A. Raduta et al., Evidence for α-particle condensation in nuclei from the Hoyle state deexcitation. Phys. Lett. B **705**(1), 65–70 (2011). https://doi.org/10.1016/j.physletb.2011.10.008
15. A. Pagano et al., Fragmentation studies with the CHIMERA detector at LNS in Catania: recent progress. Nucl. Phys. A **734**, 504–511 (2004). https://doi.org/10.1016/j.nuclphysa.2004.01.093
16. A. Badalá, M.L. Cognata, R. Nania et al., Trends in particle and nuclei identification techniques in nuclear physics experiments. La Rivista del Nuovo Cimento **45**, 189–276 (2022). https://doi.org/10.1007/s40766-021-00028-5
17. E. De Filippo, B. Gnoffo, E.V. Pagano et al., The FARCOS array at LNS. in preparation
18. L. Acosta, et al., The FARCOS detection system: the first application in a real experiment. 2019 IEEE Nuclear Science Symposium and Medical Imaging Conference (NSS/MIC) pp. 1–4 (2019). https://doi.org/10.1109/NSS/MIC42101.2019.9060013
19. E. Geraci, et al., Highlights from CHIMERA Collaboration. Il Nuovo Cimento **45 C**, 44 (2022). https://doi.org/10.1393/ncc/i2022-22044-5
20. N. Martorana, G. Cardella, E. Lanza et al., First measurement of the isoscalar excitation above the neutron emission threshold of the pygmy dipole resonance in 68ni. Phys. Lett. B **782**, 112–116 (2018)
21. G. Cardella, A. Bonasera, N. Martorana et al., Search for rare 3-α decays in the region of the Hoyle state of ^{12}C. Nuclear Phys. A **1020**, 122395 (2022). https://doi.org/10.1016/j.nuclphysa.2022.122395
22. G. Cardella, F. Favela, N.S. Martorana et al., Investigating γ-ray decay of excited ^{12}C levels with a multifold coincidence analysis. Phys. Rev. C **104**, 064315 (2021). https://doi.org/10.1103/PhysRevC.104.064315
23. A. Trifiró, et al., A laser based system for high resolution positioning of farcos array. LNS report 2020 pp. 79–80 (2021). https://www.lns.infn.it/it/download/download-history/category/35-lns-activity-report.html
24. S. Aiello et al., Timing performances and edge effects of detectors worked from 6-in. silicon slices. Nucl. Instrum. Methods Phys. Res., Sect. A **385**(2), 306–310 (1997). https://doi.org/10.1016/S0168-9002(96)00881-9
25. S. Aiello et al., Plasma effects for heavy ions in implanted silicon detectors. Nucl. Instrum. Methods Phys. Res., Sect. A **427**, 510–517 (1999). https://doi.org/10.1016/S0168-9002(98)01426-0
26. B. Gnoffo, P. Russotto, E.D. Filippo, et al., Particles identification based on the time of flight technique in chimera silicon detectors. LNS report p. 87 (2020). https://www.lns.infn.it/it/download/download-history/download/35-lns-activity-report/1184-lns-activity-report-2020.html
27. P. Russotto, et al., submitted. to NIM A
28. E. De Filippo, A. Pagano, J. Wilczyński et al., Time sequence and time scale of intermediate mass fragment emission. Phys. Rev. C **71**, 044602 (2005). https://doi.org/10.1103/PhysRevC.71.044602
29. C. Ammerlaan, R. Rumphorst, L. Koerts, Particle identification by pulse shape discrimination in the p-i-n type semiconductor detector. Nucl. Inst. Methods **22**, 189–200 (1963). https://doi.org/10.1016/0029-554X(63)90248-9
30. G. Pausch, M. Moszyński, D. Wolski, W. Bohne, H. Grawe, D. Hilscher, R. Schubart, G. de Angelis, M. de Poli, Application of the pulse-shape technique to proton-alpha discrimination in Si-detector arrays. Nucl. Instrum. Methods Phys. Res., Sect. A **365**(1), 176–184 (1995). https://doi.org/10.1016/0168-9002(95)00488-2
31. G. Prete et al., The 8πLP project at LNL. a detection system for light charged particles with deexcitation channel selection. Nucl. Instrum. Methods Phys. Res., Sect. A **422**(1), 263–268 (1999). https://doi.org/10.1016/S0168-9002(98)00954-1
32. J. Lu, P. Figuera et al., Pulse shape discrimination of charged particles with a silicon strip detector. Nucl. Instrum. Methods Phys. Res., Sect. A **471**(3), 374–379 (2001). https://doi.org/10.1016/S0168-9002(01)00805-1
33. S. Carboni, S. Barlini, L. Bardelli, N. Le Neindre et al., Particle identification using the δe-e technique and pulse shape discrimination with the silicon detectors of the fazia project. Nucl. Instrum. Methods Phys. Res., Sect. A **664**(1), 251–263 (2012). https://doi.org/10.1016/j.nima.2011.10.061
34. G. Pastore, D. Gruyer, P. Ottanelli, N. Le Neindre, G. Pasquali et al., Isotopic identification using pulse shape analysis of current signals from silicon detectors: Recent results from the FAZIA collaboration. Nucl. Instrum. Methods Phys. Res., Sect. A **860**, 42–50 (2017). https://doi.org/10.1016/j.nima.2017.01.048
35. R. Bassini, C. Boiano, A. Pagano, et al., A modular NIM electronics for Pulse Shape method with the large area n-planar silicon detectors of the 4π CHIMERA. in 2006 IEEE Nuclear Science Symposium Conference Record **1**, 507–509 (2006). https://doi.org/10.1109/NSSMIC.2006.356208

36. B. Gnoffo, Isospin influence on the IMFs production in the ^{78,86}Kr+^{40,48}Ca reactions at 10 AMeV. Il Nuovo Cimento **39 C**, 275 (2016). https://doi.org/10.1393/ncc/i2016-16275-0

37. S. Pirrone, G. Politi, B. Gnoffo et al., Isospin influence on fragments production in ^{78}Kr+^{40}Ca and ^{86}Kr+^{48}Ca collisions at 10 MeV/nucleon. Eur. Phys. J. A **55**, 22 (2019). https://doi.org/10.1140/epja/i2019-12695-4

38. M. Alderighi et al., Particle identification method in the CsI(Tl) scintillator used for the CHIMERA 4π detector. Nucl. Instrum. Methods Phys. Res., Sect. A **489**(1), 257–265 (2002). https://doi.org/10.1016/S0168-9002(02)00800-8

39. F. Amorini et al., Investigation of the dependence of CsI(Tl) scintillation time constants and intensities on particle's energy, charge and mass through direct fitting of digitized waveforms. IEEE Trans. Nucl. Sci. **59**(4), 1772–1780 (2012). https://doi.org/10.1109/TNS.2012.2201499

40. D. Horn, G. Ball, A. Galindo-Uribarri, E. Hagberg, R. Walker, R. Laforest, J. Pouliot, The mass dependence of CsI(Tl) scintillation response to heavy ions. Nucl. Instrum. Methods Phys. Res., Sect. A **320**(1), 273–276 (1992). https://doi.org/10.1016/0168-9002(92)90785-3

41. L. Acosta et al., Probing the merits of different event parameters for the identification of light charged particles in CHIMERA CsI(Tl) detectors with digital pulse shape analysis. IEEE Trans. Nucl. Sci. **60**(1), 284–292 (2013). https://doi.org/10.1109/TNS.2013.2237789

42. W. Zipper, et al., Identification of ^{8}Be isotopes in the CsI of CHIMERA detector. Proceedings, International Workshop on Multifragmentation and Related Topics (IWM 2005): Catania, Italy, November 28-December 1, 2005 pp. 115–121 (2006)

43. S. Pirrone, G. Politi, M. La Commara, J.P. Wieleczko, E. De Filippo, B. Gnoffo, et al., Decay competition in IMF production in the collisions ^{78}Kr+^{40}Ca and ^{86}Kr+^{48}Ca at 10 AMeV. J. Phys.: Conf. Ser. **515**, 012,018 (2014). https://doi.org/10.1088/1742-6596/515/1/012018

44. L. Morelli, M. Bruno, M. D'Agostino, G. Baiocco, F. Gulminelli et al., The 12c hoyle state in the inelastic 12c + 12c reaction and 24mg decay. J. Phys. G: Nuclear Particle Phys. **43**(4), 045110 (2016). https://doi.org/10.1088/0954-3899/43/4/045110

45. D. Dell'Aquila, I. Lombardo, G. Verde, M. Vigilante et al., High-precision probe of the fully sequential decay width of the Hoyle state in ^{12}C. Phys. Rev. Lett. **119**, 132501 (2017). https://doi.org/10.1103/PhysRevLett.119.132501